Biophysical Journal, Volume *115*

Supplemental Information

Single Proteoliposome High-Content Analysis Reveals Differences in the Homo-Oligomerization of GPCRs

Samuel M. Walsh, Signe Mathiasen, Sune M. Christensen, Jonathan F. Fay, Christopher King, Davide Provasi, Ernesto Borrero, Søren G.F. Rasmussen, Juan Jose Fung, Marta Filizola, Kalina Hristova, Brian Kobilka, David L. Farrens, and Dimitrios Stamou

Single proteoliposome high content analysis reveals differences in the homo-oligomerization of GPCRs

Supporting Material

S. M. Walsh, S. Mathiasen, S. M. Christensen, J. F. Fay, C. King, D. Provasi, E. Borrero, S. G. F. Rasmussen, J. J. Fung, M. Filizola, K. Hristova, B. Kobilka, D. L. Farrens, D. Stamou

Contents

1 SUPPORTING MATERIALS AND METHODS

1.1 Engineered receptor constructs

Receptor constructs were engineered with a specific cysteine labeling site for fluorescent labeling on the surface exposed part of Helix 8 (H8).

B_2AR labelled at H8 position R333C (1): This construct was termed Δ5. Five cysteines were mutated and substituted respectively with (C77V, C265A, C327S, C378A and C406A). Subsequently, a single cysteine was introduced at R333C for specific labelling.

CB_1 labelled at H8 position A407C (2): Minimal cysteine truncated purification construct (Δ88/Δ417) termed θ, in which only two of the 13 endogenous cysteines (Cys-257 and Cys-264) were retained to ensure a functional receptor (2). A specific cysteine for labelling was introduced at A407C.

Opsin labelled at Helix 8 position 316C (3, 4): The construct termed θ' was created using a well characterized non-reactive labelling construct (140S, 167S, 222S, 264S, 322S, and 323S) (4). Into this construct two cysteines were introduced (N2C, D282C) to thermally stabilize the apo protein opsin (3). The endogenous 316C was used for specific labelling.

1.2 Orientation of receptors

The orientation of β_2AR was previously determined by Fung et al. (1) to be ~90% outside out. The orientation of CB_1 and opsin was determined by digestion of the receptors C-terminal region with V8 protease and the concurrent loss of the rhodopsin 1D4 epitope (TETSQVAPA) (5). The 1D4 epitope was used to aid in receptor purification (see (5)). Immunoblot analysis with the 1D4 monoclonal antibody in **Fig. S1** shows that CB_1 and opsin are orientated with the extracellular domain inside the proteoliposome (inside out).

1.3 Determining fluorescent signal correction factors (ω, α, β)

To accurately determine $E_{FRET,}$ fluorescent signals were carefully corrected for fluorescence contaminations using correction factors (ω, α, β) (see **Quantification of E_{FRET} (Materials and Methods)**). We used three control samples (preparations 2-4 described in **Proteoliposome preparation (Materials and Methods))** and imaged these employing the exact same microscopy conditions as for the proteoliposomes investigated for FRET (preparation 1). Correction factors were determined separately for β_2AR and for CB_1 and opsin samples to account for smaller changes in the microscope alignments and to accommodate a potential requirement for re-optimization of laser and image settings. All correction factors are reported as mean ± sem determined from hundreds (n) of single proteoliposomes. In the following section superscript ^{0} denotes raw uncorrected intensities. I_D and $I_A^{0,FRET}$ are the donor and acceptor intensity excited by the donor laser line (543 nm).

ω was determined using the control sample labeled only by OG-DHPE (preparation 2) and represents the ratio of OG intensity in the I_D^0 channel to OG intensity in the membrane channel (I_M^0) when excited with the 476 nm laser. ω was determined to be 0.9 ± 0.02% for β_2AR (n = 729) (13) and (3.3 ± 0.0004%) (n = 1163) for CB_1 and opsin.

β was determined using the control sample harboring only GPCR-Cy3 (preparation 3) and represents the ratio of Cy3 intensity in the acceptor emission channel to Cy3 intensity in the donor emission channel when excited with the 543 nm laser. β was determined to be (11.1 ± 0.06%) for β_2AR (n = 1130) (13), (14.5 ± 0.001%) for CB_1 (n = 1399) and (13.3 ± 0.001%) for opsin (n = 1630).

α was determined using the control sample harboring GPCR-Cy5 only (preparation 4) and represents the ratio of Cy5 intensity in the acceptor channel when excited by the 543 nm laser to the intensity of Cy5 intensity in the acceptor channel excited by the 633 nm laser. α was determined to be (9.8 ± 0.1%) for β_2AR (n = 1130) (13), (6.7 ± 0.001%) for CB_1 (n = 1399) and (6.2 ± 0.001%) for opsin (n = 1630).

1.4 Proteoliposome size

Proteoliposome diameters were determined as described previously (6, 9, 10) by relating the fluorescence intensity of the proteoliposome membrane fluorophore OG-DHPE to proteoliposome diameter as measured by dynamic light scattering (DLS). Briefly, because the number of fluorophores incorporated in the membrane (Oregon Green-DHPE) is proportional to the proteoliposome surface area and thereby related to diameter (D) through Eq. S1, a conversion from diffraction limited intensity spots to physical proteoliposome size was possible.

$$I_{Oregon\ Green\ DHPE} \propto A_{Liposome} = \pi D_{Liposome}^2$$
$$\Rightarrow D_{Liposome} = C_{cal}\sqrt{I_{Oregon\ Green\ DHPE}} \qquad [S1]$$

The calibration factor (C_{cal}) was determined by the use of a calibration sample, where empty liposomes were extruded 20× through two 50 nm filters (Millipore) to produce a narrow size distribution. The calibration sample was first examined by DLS to obtain a mean diameter, and then by confocal microscopy utilizing identical imaging conditions as for GPCR-Cy3 and GPCR-Cy5 (preparation 1). The mean of the integrated Oregon Green-DHPE intensity spots was correlated to the mean radius found by DLS to obtain C_{cal}. When C_{cal} was determined all intensities were converted to diameters by Eq. S1. DLS measurements were performed on an ALV-5000 correlator equipped with a 633 nm laser. The concentration of liposomes was 0.1 g/l, and all data were collected at room temperature.

1.5 Receptor density

To calibrate receptor densities we used the fluorescent intensities from either control samples harboring only GPCR-Cy3 (preparation 3) and only GPCR-Cy5 (preparation 4) and the calculated single proteoliposome surface area. The integrated intensity of the labeled receptor $I_{A/D}$ is proportional to the number of fluorophores, and thus the number of proteins, since each receptor carries one label. This holds true for acceptor fluorophores excited by acceptor laserline (633 nm) however donor intensities are quenched by FRET. To recover the unquenched donor intensity we added the corrected acceptor FRET intensity to I_D (7), using an I_A^{FRET} that was decoupled from instrumental and photo-physical effects through the γ-factor.

We collected single molecule bleaching traces for control samples preparation 3 and preparation 4. Bleaching movies were acquired on a Leica DMI6000 TIRF setup using an oil

immersion objective HCX PL APO CS (100× magnification, 1.46 NA) (Leica). Oregon Green-DHPE, GPCR-Cy3 and GPCR-Cy5 were excited by a 488 nm laserline, a 561 nm laserline and a 635 nm laserline respectively. Oregon Green emission was filtered through a filtercube with a dichroic mirror Q495LP and a bandpass filter HQ525/50m. Cy3 emission was filtered through a filtercube with a dichroic mirror T565LP and a bandpass filter ET605/70m. Cy5 emission was filtered through a filtercube with a dichroic mirror Q660LP and a bandpass filter HQ700/75m. All filters and dichroic mirrors were from Chroma Technology. The fluorescence intensity was collected on an electron-multiplying Andor Ixon 897 camera. Images were acquired in the format of 512×512 pixels, each pixel corresponding to 160 nm sample length, bit-depth of 14 and 250 ms exposure time. Each frame was transferred in 0.304 s, bleaching series were acquired for 900 frames. Single molecule bleaching trace intensities were extracted by software written in Igor Pro Ver. 6.01 (Wavemetrics). Single molecule bleaching step intensities were quantified by subtracting the average step intensity by the average background intensity (6). For a narrow size distribution ranging from $0-60$ nm the mean number of receptor, were assessed by dividing the unbleached starting intensity by the mean bleaching step intensity (11). The mean number of receptors was correlated to the mean intensity obtained by confocal microscopy for the same narrow size range ($0-60$ nm) and this factor was used to access the number of receptors on all individual proteoliposomes.

1.6 Ensemble proteoliposome E_{FRET}

To determine the ensemble average E_{FRET} we composed a pseudo FRET efficiency by summing up all intensity signals from the imaged proteoliposome samples including signals from protein aggregates and proteoliposomes carrying only donor or acceptor labeled receptors using Eq. S2.

$$E_{bulk}^{FRET} = \frac{\frac{1}{N}\sum_N I_A^{FRET} - \beta\frac{1}{N}\sum_N I_D - \alpha\frac{1}{N}\sum_N I_A}{\frac{1}{N}\sum_N I_A^{FRET} - \beta\frac{1}{N}\sum_N I_D - \alpha\frac{1}{N}\sum_N I_A + \frac{1}{N}\sum_N I_D} \quad [S2]$$

1.7 Error propagation

The uncertainty associated with quantifying proteoliposome diameter, receptor densities, A/D ratios, and E_{FRET} were determined as described previously (6). Briefly, we propagated the errors on the 2D Gaussian fit coefficients used to determine the fluorescence intensity of each single

particle (see **Single fluorescent particle characterization (Materials and Methods)**). In **Fig. 1** ***D-G*** the full width of the propagated error histograms for the GPCR with the largest errors are shown.

1.8 Average monomer distance

We assumed receptors to be monomeric and equally distributed in the proteoliposomes. We determined the average distance between any two receptors in 3D for proteoliposomes with the highest and lowest densities. The smallest proteoliposome (40 nm diameter) with the highest density (3.0×10^{-3} receptors/nm^2) gave an average distance between any two receptors of 17 nm. Likewise, the largest proteoliposome (400 nm diameter) with the lowest observed density (0.3×10^{-3} receptors/nm^2) gave an average distance between two receptors of 58 nm.

1.9 Total receptor per assay

To estimate the total amount of receptor needed for a miniaturized screen, we used the fact that a microscope experiment required 1.5 × 106 liposomes given a microscope chamber of 5 mm in diameter and a surface density of 7.5 × 1010 proteoliposomes/m^2. Assuming each liposome carries 50 receptors of 47,058.1 g/mol each, this corresponds to 5.9 pg of protein.

1.10 Ligands

Proteoliposomes containing reconstituted β_2AR were incubated with saturating amounts (10 μM) of agonist Isoproterenol (ISO) (Sigma), and saturating amounts (500 nM) of inverse agonist ICI 118,551 (Sigma). Samples were incubated with ligands for 30 min at room temperature before measurements were taken.

1.11 Receptor stoichiometry

Using the oligomer stoichiometry theory proposed by Veatch and Stryer (12), in a modified version (13), we relate E_{FRET} to the A/D ratio and extract the apparent average oligomer stoichiometry as a fitting parameter. Here stoichiometry (n) is related to energy transfer (E_{FRET})

and maximum FRET efficiency $E_{FRETmax}$, and the mole fraction of the acceptor is represented as the acceptor to donor mole ratio (A/D ratio):

$$E_{FRET} = (1 - \frac{1}{(1+(\text{A/D ratio}))^{n-1}}) * E_{FRETmax} \quad \text{[S3]}$$

Data were fit using the Curve Fitting Toolbox in MATLAB v. 8.2 (MathWorks Inc.) evaluating *n* and $E_{FRETmax}$ as free fitting parameters. The fit was weighted with the propagated A/D ratio errors (described in **Error Propagation**).

The apparent average stoichiometry as a function of density (**Fig. 2** ***C***) only included proteoliposomes within ± 15 nm of the mean proteoliposome diameter (see **Table S1**) to avoid convoluting the effect of density with membrane curvature. The apparent average stoichiometry as a function of membrane curvature (**Fig. 3** ***B*** and **Fig. S3**) only included proteoliposomes within ± 0.2 × 10^{-3} receptors/nm^2 of the mean receptor density to avoid convoluting the effect of membrane curvature with total receptor density.

1.12 Receptor association energies

The FRET efficiencies of donor-labeled and acceptor-labeled protein oligomers were calculated using the "kinetic theory of FRET", as derived by Raicu (14, 15):

$$E_{oligo}^{Dq} = \frac{\mu_{oligo}}{[D]_T} \sum_{k=1}^{n-1} \frac{k(n-k)\tilde{E}}{1+(n-k-1)\tilde{E}} \binom{n}{k} P_D^k P_A^{n-k} \quad \text{[S4]}$$

In Eq. S4, n represents the oligomer order. μ_{oligo} is the concentration of oligomers. P_D and P_A are the fractions of donors and acceptors in the oligomer. For large numbers of molecules, P_D and P_A are equal to the fraction of donor and acceptors, respectively: x_D and x_A. $x_A = \frac{[A]}{[D]+[A]}$, with [D] and [A] representing the donor and acceptor concentrations, and $x_D + x_A = 1$. Only proteoliposomes having diameters between 120 − 130 nm were selected to avoid convoluting geometric curvature with oligomeric fraction.

Eq. S4 gives the theoretical apparent donor-quenched energy transfer efficiency for mixtures of monomers and oligomers, assuming an equal donor to acceptor distance for all D-A pairs in the oligomer. For the case of n = 2, a dimer, this is always correct as there is only one donor and one acceptor in the dimer pair. For trimers and above, this is an approximation which minimizes the number of adjustable parameters in the theoretical model for FRET (16). We fit Eq. S4 for n = 2 (β_2AR) and n = 4 (CB_1 and opsin), corresponding to the cases of monomer-dimer and monomer-

tetramer thermodynamic equilibria, to the experimental data as described below. Because CB_1 was found to form a mixture of oligomers from 2.8 ± 0.6 to 5.3 ± 0.6 in proteoliposomes with diameters between 120 – 130 nm (**Fig. 2 *C***), we chose to fit CB_1 using the average stoichiometry in this proteoliposome diameter range corresponding to a monomer-tetramer model. We determined the minimized chi-squared value for all oligomeric models. The kinetic model for FRET, however, does not take into account stochastic FRET, or FRET that occurs due to random approach of donors and acceptors in the membrane within distances of ~100 Å (14, 17). Stochastic FRET can represent a significant contribution to measured E_{FRET} in the case of a monomer-dimer equilibrium, but it decreases significantly as a function of oligomer size. As such, here we corrected for stochastic FRET in the dimer case (see (18) for details), but we did not apply a proximity FRET correction for higher order oligomers. FRET for a mixed population of monomers and dimers can be modeled as a function of the dimeric fraction $f_d(K_A,[T])$ according to Eq. S5:

$$E_{dimer}^{Dq} = f_D(K_A,[T])\, x_A \tilde{E} \quad [S5]$$

To this FRET prediction, we added a contribution for stochastic FRET (18) and completed the theoretical model for the apparent FRET efficiency for the case of a monomer-dimer equilibrium (17, 18):

$$E_{app,theory,i} = E(K_A,[A]_i)_{proximity} + x_{A,i} f_D(K,[T]_i)\tilde{E} \quad [S6]$$

Next, we vary the $\tilde{E}$ and K values, and we choose the model which minimizes the chi-squared as the best model to represent the data (16). The chi-squared value is calculated according to:

$$\chi^2(K,\tilde{E}) = \frac{1}{N-2-1}\sum_{i=1}^{N\ data\ points}\left(\frac{E_{app,theory,i} - E_{app,i}}{\sigma_i}\right)^2 \quad [S7]$$

We followed the same basic procedure for fitting of higher order oligomerization models, except that there was no proximity FRET correction: $E_{app} \approx E_{oligo}^{Dq}$. As discussed above, this approximation is justified as the stochastic FRET contribution to the signal decreases significantly as a function of oligomer order (18).

To record the fraction of oligomers as a function of total concentration and an equilibrium association constant for the association of n monomers to an n'th order oligomer, $n * [m] \rightleftharpoons oligo$, one must find the roots of an n'th order equation. Instead of finding the analytical solution

for the fraction of oligomers as a function of total receptor concentration, which is impossible for n > 5, we utilized a MATLAB root finding function to numerically calculate the roots of the binding polynomial. We took the largest real root as the physical solution to the n'th order polynomial which yields [m_i] as a function of K_A and [T_i]. As with the case of the monomer-dimer equilibrium, we varied the $\tilde{E}$ and K values, and we chose the model which minimized the chi-squared as the best-fit model to represent the data (Eq. S7).

Having determined the association constants of oligomerization for β_2AR ($8.3 \pm 0.9 \times 10^2$ dimer/receptor^2) and for CB_1 ($2.0 \pm 1.0 \times 10^{11}$ tetramer/receptor^4), we could then calculate the apparent Gibbs free energy of association (ΔG_a) by:

$$\Delta G_a = -RTln(K_a) \quad [S8]$$

where R is the universal gas constant, and T is temperature in Kelvin (T = 293±14 K).

1.13 Estimation of β_2AR association energies as a function of membrane curvature

Previously (6), we determined the standard Gibbs free energy of association to be -4.66 ± 0.24 kcal/mole (-8 k_BT) for proteoliposomes of 120 – 130 nm in diameter. In this study we utilized a theoretical scheme (17) that describes the FRET efficiency of dimerizing receptors in a 2D membrane environment based on two contributions: a) the efficiency arising from random collisions and b) the efficiency arising from dimerized proteins. An analytical approximation of the FRET efficiency for a random distribution of donors and acceptors in a 2D membrane is given by (17)

$$E_{Random} = 1 - (A_1 e^{-k_1 C_a} + A_2 e^{-k_2 C_a}) \quad [S9]$$

Here the concept of reduced acceptor density (C_a) is introduced as the acceptor surface density multiplied by a Förster radius (R_0) area (R_0^2)(For Cy3/Cy5 R_0=53 Å (19)). $A_{1,2}$ and $k_{1,2}$ are constants that vary for different values of (R_e/R_0), R_e being the closest approach between donor and acceptor when attached to receptors. Based on structural information R_e/R_0 was assumed to be 1 (20) for reconstituted β_2AR. For a system including dimerized donors and acceptors, the FRET efficiency is given by

$$E_{FRET} = (1 - f_b)E_{Random} + f_b E_{Bound} \quad [S10]$$

where E_{bound} is the FRET efficiency within a dimer. E_{bound} is weighted by the fraction of bound donors (f_b), as the probability that a randomly chosen donor is bound to an acceptor. f_b can be expressed as the probability that a single randomly chosen donor will be in a dimer (f_d) multiplied by the probability that the second unit in the dimer is an acceptor (P_A) (21). P_A is expressed in terms of reduced donor and acceptor densities as $C_a/(C_a+C_d)$.

$$E_{FRET} = (1 - f_d P_A)E_{Random} + f_d P_A E_{Bound} \quad [S11]$$

The fraction of dimers can thus be expressed as

$$f_d = \left(\frac{E_{FRET} - E_{Random}}{E_{bound} - E_{Random}}\right)\frac{1}{P_A} \quad [S12]$$

Because both acceptor density and total receptor density is constant in the analysis performed here (see **Fig. S3 *D***), E_{random} and P_A are constant. Assuming that E_{bound} remains unchanged with curvature, and utilizing the E_{bound} obtained for β_2AR (~0.2), we can therefore calculate the fraction of dimers for each curvature, employing the measured E_{FRET} (**Fig. 3 *A***).

For a monomer dimer equilibrium, $[M] + [M] \leftrightarrow [D]$, the association constant is given by

$$K_a = \frac{[D]}{[M]^2} \quad [S13]$$

As pointed out by Fleming *et al* (22) it is crucial for a correct thermodynamic description of protein association in a hydrophobic solute to apply the effective concentration of proteins in the lipid phase. This is in contrast to, for example, protein concentration in the total volume of buffer and lipids. In accordance with this we employed the mole fraction scale, permitting extraction of a standard Gibbs free energy that can be directly compared to reported literature values. The fraction of dimers can be expressed in terms of K_a and the total receptor mole fraction X_p according to (23)

$$f_d = \frac{4K_aX_p + 1 - \sqrt{8K_aX_p + 1}}{4K_aX_p} \quad [S14]$$

where (X_p) is given by

$$X_P = \frac{2N_{protein}}{2N_{protein} + N_{lipids}} = \frac{2N_{protein}}{2N_{protein} + 2\frac{A_{liposome}}{A_{lipid}}} \quad [S15]$$

$N_{protein}$ and N_{lipids} being the numbers of receptors and lipids respectively and two accounting for the transmembrane nature of the receptors. Due to the lipid bilayer N_{lipids} is given by twice the liposome area ($A_{liposome}$) divided by the lipid headgroup area (A_{lipid}= 0.67 nm^2) (24).

Isolating K_a in Eq. S16 yields a solution given by

$$K_a = \frac{f_d}{2X_p(f_d - 1)^2} \quad [S16]$$

Hence, from the calculated fraction of dimers we obtain a K_a at the molefraction scale for each curvature, and finally a standard Gibbs free association energy according to Eq. S8. K_a obtained on the molefraction scale is converted to units of copies/Area according to the scheme published by Provasi *et al.* (25) using a lipid headgroup area of 0.67 nm^2 (24).

1.14 Calculation of β_2AR on-rates

A prototypical model for diffusion of cylindrical inclusions in membranes is the Saffman-Delbrück model (26), which treats the membrane as a 2D viscous fluid with two dimensional viscosity $\eta_m = h\nu_m$, h being thickness and ν_m the lipid viscosity, surrounded by a 3D ("embedding") fluid with three dimensional viscosity ν_w. The diffusion of a cylindrical inclusion of radius a is given by $D_{SD} = D_0 / 4\pi\ (\ln(2\xi_0/a_c) - \gamma)$, where a_c is the protomer radius, γ the Euler-Mascheroni constant, $D_0 = k_BT/\eta_m \sim 10$ nm^2/μs sets the units for the diffusion constant and $\xi_0 = \eta_m/(2\nu_w)$ is the Saffman-Delbrück length, i.e. the characteristic scale beyond which the membrane exchanges in-plane momentum with the surrounding fluid. This model is derived from hydrodynamic considerations for the 2D flat slab surrounded by the embedding solvent. Using ν_w ~1cP and ν_m~1P gives ξ_0=200 nm.

Generalizing this to the spherical case (27), the co-rotational diffusion of the inclusion of particles in liposomes – that is the mobility of the proteins with respect to the vesicle – is given by:

$$D_{co-rot} = \frac{D_0}{8\pi} \sum_{l=2}^{l_{max}} \frac{2l+1}{s_l} \quad [S17]$$

$s_l = l(l+1) - 2 + 2R/\xi_0\ (2l+1)$, R being the vesicle radius.The cutoff $l_{max} = \exp(-\gamma)\ 2R/a_c$ was introduced to regularize a high-momentum divergence and was chosen so that the for vanishing

curvature, Eq. S15 gives the flat Saffman-Delbrück result. The diffusion for proteins (a_c ~ 3.0 nm) in vesicles of different diameters estimated with Eq. S17 are plotted in **Fig. 3** ***D***. To convert this diffusion into a dimerization rate, we assumed a diffusion-limited dimerization step, and used the Smoulchowski theory in 2D to obtain the on-rate k_{on}

$$k_{on}(D_c) = \frac{4\pi D_c}{\ln\left(\frac{4\pi D_c t_{exp}}{a_c^2}\right) - \gamma} \quad [S18]$$

where t_{exp} refers to typical experimental time scales explored to detect diffusion, and D_c is the diffusion constant of the protomers. Combined, Eq. S17 and Eq. S18 allowed us to calculate the on-rate as a function of the membrane curvature (see **Fig. 3** ***D***).

2 SUPPORTING FIGURES AND TABLES

2.1 Supporting Figure 1

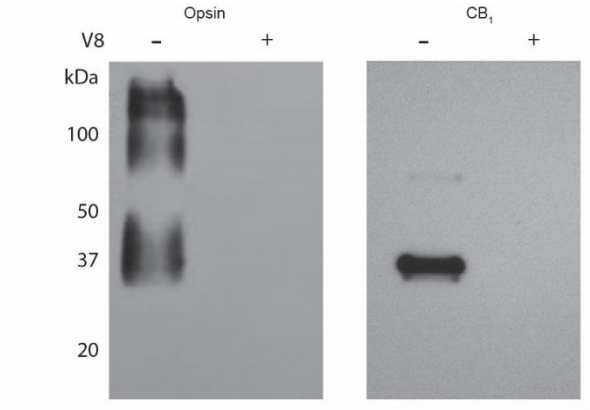

Orientation of CB1 and opsin in proteoliposomes. To assess the orientation of the receptor in proteoliposomes, we tested proteoliposome samples for their susceptibility to proteolysis by V8 protease. The V8 protease can cleave opsin and our CB1 purification mutant at the C-terminus, causing a loss of the 1D4 epitope. For digestion to occur the cytoplasmic face must be exposed (i.e. on the outside of the vesicles). Immunoblot analysis with an anti C-terminal antibody (1D4, that binds to both opsin and our CB1 purification mutant) showed that liposome samples incubated with V8 protease (+) show a loss of epitope binding compared to samples without V8 protease incubation (-). The immunoblot in **Fig. S1** reveals that the vast majority of CB1 and opsin samples are oriented inside-out.

2.2 Supporting Figure 2

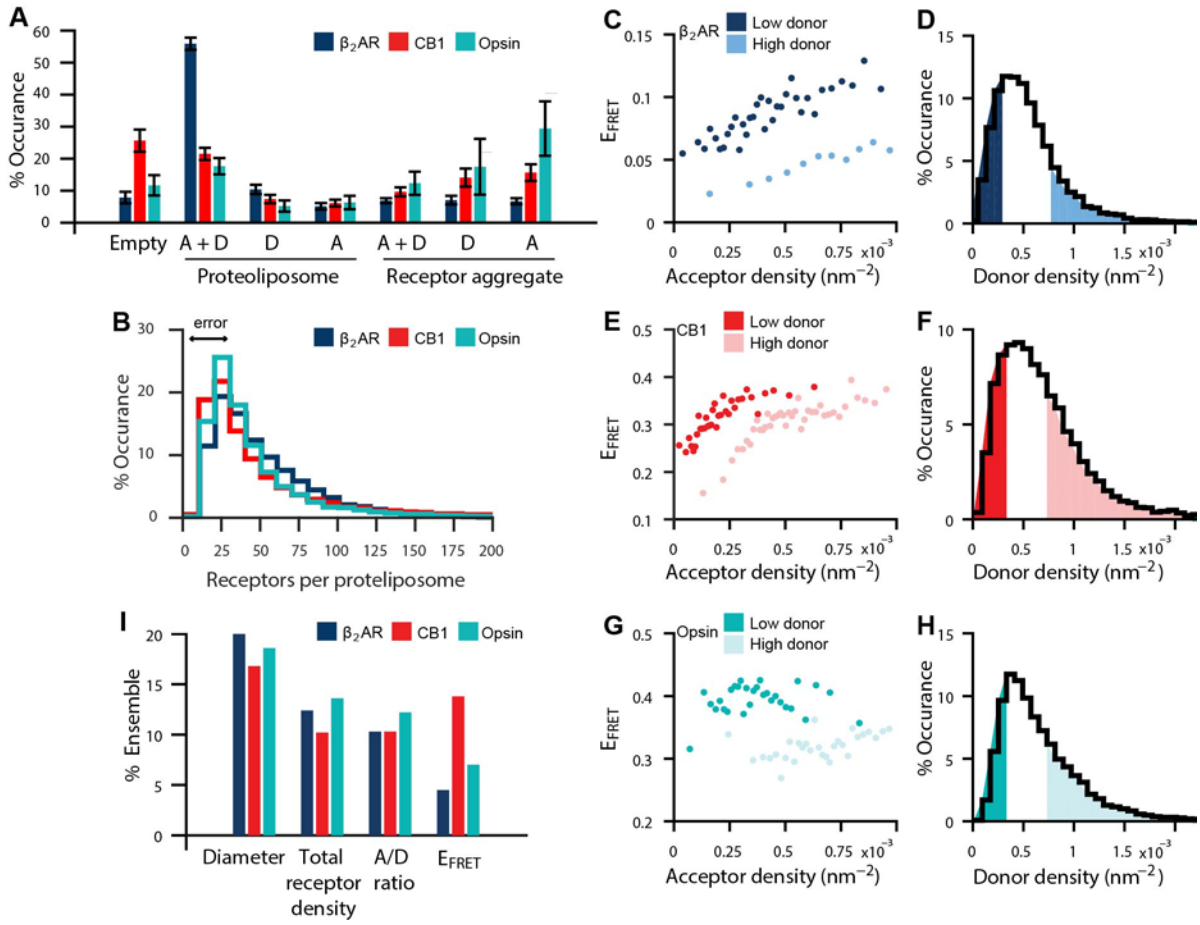

Characterization of proteoliposome samples. (**A**) Particle subpopulations within GPCR reconstituted proteoliposome samples included empty proteoliposomes (Empty), proteoliposomes with both donor and acceptor (A+D), only donors GPCR (D) and only acceptors (A) labeled GPCRs, and receptor aggregates of only donor (D), only acceptors (A), and donor and acceptor (A+D) labeled GPCRs. For each GPCR the total number of single particles included in the analysis comprises n > 9000 single particles. Data is shown as a weighted average with uncertainties representing the standard deviation of technical replicates from 3 independent experiments. (**B**) Histogram displaying of the number of receptors in individual (A+D) proteoliposomes. For each GPCR data comprise n > 12800 single proteoliposomes from > 5 technical replicates. Error shown represents the full width of the propagated error histogram for the GPCR with the largest error. (**C-H**) E_{FRET} is specific and not due to stochastic interactions. (**C, E, G**) We plot E_{FRET} as a function of total acceptor density at a low ($0 – 0.3 \times 10^{-3}$ receptors/nm^2) and high ($0.8 – 10 \times 10^{-3}$ receptors/nm^2) total donor density. Because we see a relative increase of E_{FRET} at lower total density of donor we conclude that FRET is a result of specific interaction of GPCR monomers and is not due to by-stander FRET (28). Data in **C, E, G** were binned (100 single proteoliposomes per bin) and a weighted average shown. For each GPCR and each donor density selection (low or high) data n > 1100 single proteoliposomes. Uncertainties are less than or equal to the displayed marker size. Proteoliposomes selected for analysis in **C, E, G** are shown in panels (**D, F, H**) as a histogram of total donor density. (**I**) To determine how representative ensemble averages were of the underlying single proteoliposome population, we counted the number of single proteoliposomes which fell within the ensemble average ± 10%. Data are shown as a percentage of the total number of single proteoliposomes (see **Table S1**). **Fig. S2** shows that (1) proteoliposome reconstitutions contain significant percentage of unintended particles, (2) E_{FRET} is specific in selected proteoliposomes and is not dominated by

bystander FRET, (3) ensemble proteoliposome measurements do not represent the underlying single proteoliposome population.

2.3 Supporting Figure 3

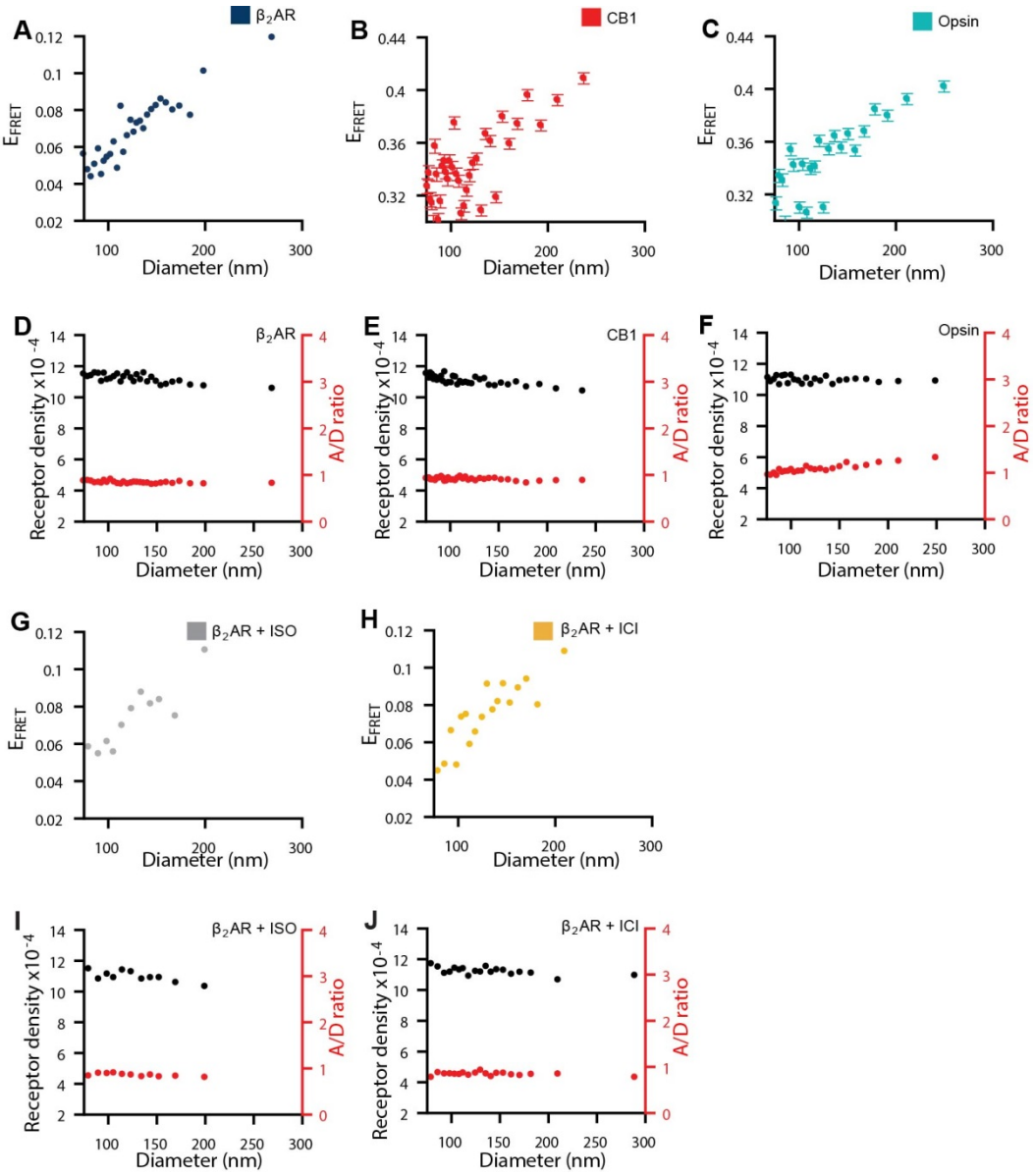

Membrane curvature reduces the oligomerization of GPCRs. (**A-C**) GPCR oligomerization increases as proteoliposome diameter (and planarity) increases. Data in **A-C** were selected for constant donor and acceptor GPCR densities ($0.4 - 0.8 \times 10^{-3}$ receptors/nm^2) and were binned (75 proteoliposomes per bin) with weighted average shown. Data in **A-C** comprise n > 1800 single proteoliposomes. (**D-F**) Controls showing that neither total receptor density (black) nor the A/D ratio (red) vary with proteoliposome diameter. (**G-H**) Response of β_2AR to the agonist Isoproterenol (ISO) or the inverse agonist ICI 118,551 (ICI) at saturating conditions. Ligands do not modify the response of β_2AR to

membrane curvature. Data in **G-H** were selected for constant donor and acceptor GPCR densities ($0.4 - 0.8 \times 10^{-3}$ receptors/nm^2) and were binned (75 proteoliposomes per bin) with a weighted average shown. Data in **G-H** comprise n = 1575 (β_2AR + ICI) or n = 975 (β_2AR + ISO) single proteoliposomes. (**I-J**) Controls showing that neither total receptor density (black) nor the A/D ratio (red) vary with liposome diameter. Uncertainties represent the standard error of the mean and are shown in **B-C** where the uncertainties were larger than the marker size; all other uncertainties are equal to or smaller than marker size shown. Data in **A, G, H** are re-plotted from **Fig. 4** ***A***. **Fig. S3** shows that high membrane curvature decreases GPCR oligomerization.

2.4 Supporting Figure 4

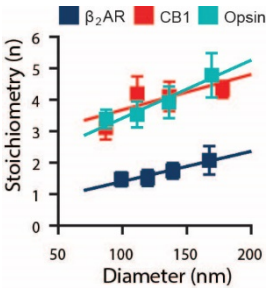

Membrane curvature decreases oligomer stoichiometry. Stoichiometry analysis repeated as in **Fig. 2** ***A*** for proteoliposomes with defined proteoliposome diameters, while maintaining a constant receptor density within $\pm 0.2 \times 10^{-3}$ receptors/nm^2 of the mean (see **Table S1**). The average stoichiometry from each diameter selection is shown. For each GPCR data comprises n > 2500 single proteoliposomes where uncertainties represent ± 1 standard deviation calculated from the fit of Eq. S3. A linear fit to each data set is included to aid interpretation. Data for β_2AR are re-plotted from **Fig. 3** ***B***. **Fig. S4** shows that the stoichiometry decreases in proteoliposomes of low diameters, hence high membrane curvatures.

2.5 Supporting Table 1

		Ensemble	Single Proteoliposome			% Ensemble
Variable	Sample		Mean	STDEV	SEM	
Proteoliposome diameter	β_2AR	101.1	114.5	45.9	0.4	20.0
	CB_1	90.6	125.5	63.0	0.5	16.8
	Opsin	81.8	105.5	48.0	0.4	18.6
Total receptor density (nm^{-2})	β_2AR	1.71×10^{-3}	1.26×10^{-3}	0.8×10^{-3}	0.7×10^{-5}	12.4
	CB_1	1.71×10^{-3}	1.11×10^{-3}	0.8×10^{-3}	0.6×10^{-5}	10.2
	Opsin	1.71×10^{-3}	1.29×10^{-3}	0.7×10^{-3}	0.6×10^{-5}	13.6
A/D Ratio	β_2AR	1.0	1.99	1.79	0.02000	10.3
	CB_1	1.0	0.82	0.54	0.00004	10.3
	Opsin	1.0	1.24	0.76	0.00600	12.2
E_{FRET}	β_2AR	0.27	0.13	0.14	0.001	4.5
	CB_1	0.27	0.34	0.15	0.001	13.8
	Opsin	0.22	0.37	0.16	0.001	7.0

Characterization of proteoliposomes using bulk or single particle approaches. Ensemble measurements or estimates were determined from starting preparation constituents or from averaging all reconstitutional particles. Briefly, ensemble average proteoliposome diameters were determined by averaging the size of all proteoliposomes with and without reconstituted receptor from the single proteoliposome assay. Ensemble average total receptor density (nm^{-2}) were estimated from a 1:1000 receptor to lipid ratio, assuming no lipid or receptor loss, and a lipid head group area of 0.67 nm^2. Ensemble average A- to D-labeled GPCRs (A/D ratio) were estimated from a 1:1 stoichiometry during receptor reconstitution. Ensemble E_{FRET} was determined by summing all fluorescent intensity signals (Methods). Single proteoliposome data represent the means, standard deviations (STDEV), and standard error of the means (SEM) from histograms presented in **Fig. 1** ***D-G*** fit with either a lognormal (total receptor density (nm^{-2}), A/D ratio, and proteoliposome diameter) or normal (E_{FRET}) distributions. The % ensemble represents the percentage of single proteoliposomes for each GPCR having values within ± 10% of the mean predicted by the bulk data. We chose 10% as a reasonable error on the bulk data based on previous reports of RET oligomerization measurements of GPCRs in proteoliposomes (1) and live cells (29).

3 SUPPORTING REFRENCES

1. Fung, J. J., X. Deupi, L. Pardo, X. J. Yao, G. A. Velez-Ruiz, B. T. DeVree, R. K. Sunahara, and B. K. Kobilka. 2009. Ligand-regulated oligomerization of β2-adrenoceptors in a model lipid bilayer. EMBO J. 28:3315-3328.
2. Fay, J. F., T. D. Dunham, and D. L. Farrens. 2005. Cysteine residues in the human cannabinoid receptor: only C257 and C264 are required for a functional receptor, and steric bulk at C386 impairs antagonist SR141716A binding. Biochemistry 44:8757-8769.
3. Ridge, K. D., Z. Lu, X. Liu, and H. G. Khorana. 1995. Structure and function in rhodopsin. Separation and characterization of the correctly folded and misfolded opsins produced

on expression of an opsin mutant gene containing only the native intradiscal cysteine codons. Biochemistry 34:3261-3267.
4. Xie, G., A. K. Gross, and D. D. Oprian. 2003. An opsin mutant with increased thermal stability. Biochemistry 42:1995-2001.
5. Fay, J. F., and D. L. Farrens. 2012. A key agonist-induced conformational change in the cannabinoid receptor CB1 is blocked by the allosteric ligand Org 27569. J. Biol. Chem. 287:33873-33882.
6. Mathiasen, S., S. M. Christensen, J. J. Fung, S. G. Rasmussen, J. F. Fay, S. K. Jorgensen, S. Veshaguri, D. L. Farrens, M. Kiskowski, and B. Kobilka. 2014. Nanoscale high-content analysis using compositional heterogeneities of single proteoliposomes. Nat. Methods 11:931-934.
7. Periasamy, A., H. Wallrabe, Y. Chen, and M. Barroso. 2008. Quantitation of protein–protein interactions: confocal FRET microscopy. Method Cell Biol. 89:569-598.
8. McCann, J. J., U. B. Choi, L. Zheng, K. Weninger, and M. E. Bowen. 2010. Optimizing methods to recover absolute FRET efficiency from immobilized single molecules. Biophys. J. 99:961-970.
9. Bendix, P. M., M. S. Pedersen, and D. Stamou. 2009. Quantification of nano-scale intermembrane contact areas by using fluorescence resonance energy transfer. Proc. Natl. Acad. Sci. U.S.A. 106:12341-12346.
10. Kunding, A. H., M. W. Mortensen, S. M. Christensen, and D. Stamou. 2008. A fluorescence-based technique to construct size distributions from single-object measurements: application to the extrusion of lipid vesicles. Biophys. J. 95:1176-1188.
11. Ulbrich, M. H., and E. Y. Isacoff. 2007. Subunit counting in membrane-bound proteins. Nature methods 4:319-321.
12. Veatch, W., and L. Stryer. 1977. The dimeric nature of the gramicidin A transmembrane channel: conductance and fluorescence energy transfer studies of hybrid channels. J. Mol. Biol. 113:89-102.
13. James, J. R., M. I. Oliveira, A. M. Carmo, A. Iaboni, and S. J. Davis. 2006. A rigorous experimental framework for detecting protein oligomerization using bioluminescence resonance energy transfer. Nat. Methods 3:1001-1006.
14. Raicu, V. 2007. Efficiency of resonance energy transfer in homo-oligomeric complexes of proteins. J. Biol. Phys. 33:109-127.
15. Patowary, S., L. F. Pisterzi, G. Biener, J. D. Holz, J. A. Oliver, J. W. Wells, and V. Raicu. 2015. Experimental Verification of the Kinetic Theory of FRET Using Optical Microspectroscopy and Obligate Oligomers. Biophys. J. 108:1613-1622.
16. Press, W. H., Flannery, B. P. , Teukolsky, S. A. , Vetterling, W. T. . 1989. Numerical Recipies. The Art of Scientific Computing. Cambridge University Press, Cambridge.
17. Wolber, P., and B. Hudson. 1979. An analytic solution to the Förster energy transfer problem in two dimensions. Biophys. J. 28:197-210.
18. King, C., S. Sarabipour, P. Byrne, D. J. Leahy, and K. Hristova. 2014. The FRET signatures of noninteracting proteins in membranes: simulations and experiments. Biophys. J. 106:1309-1317.
19. Mansoor, S. E., K. Palczewski, and D. L. Farrens. 2006. Rhodopsin self-associates in asolectin liposomes. Proc. Natl. Acad. Sci. U.S.A. 103:3060-3065.

20. Kenworthy, A., and M. Edidin. 1998. Distribution of a glycosylphosphatidylinositol-anchored protein at the apical surface of MDCK cells examined at a resolution of< 100 Å using imaging fluorescence resonance energy transfer. J. Cell Biol. 142:69-84.
21. Adair, B. D., and D. M. Engelman. 1994. Glycophorin A helical transmembrane domains dimerize in phospholipid bilayers: a resonance energy transfer study. Biochemistry 33:5539-5544.
22. Fleming, K. G. 2002. Standardizing the free energy change of transmembrane helix–helix interactions. J. Mol. Biol. 323:563–571.
23. Yano, Y., and K. Matsuzaki. 2006. Measurement of thermodynamic parameters for hydrophobic mismatch 1: self-association of a transmembrane helix. Biochemistry 45:3370-3378.
24. Marrink, S. J., A. H. De Vries, and A. E. Mark. 2004. Coarse grained model for semiquantitative lipid simulations. J. Phys. Chem. B: Cond. Phase 108:750-760.
25. Provasi, D., J. M. Johnston, and M. Filizola. 2010. Lessons from free energy simulations of δ-opioid receptor homodimers involving the fourth transmembrane helix. Biochemistry 49:6771-6776.
26. Saffman, P., and M. Delbrück. 1975. Brownian motion in biological membranes. Proc. Natl. Acad. Sci. U.S.A. 72:3111-3113.
27. Henle, M. L., and A. J. Levine. 2010. Hydrodynamics in curved membranes: The effect of geometry on particulate mobility. Phys. Rev. E 81:011905.
28. Lan, T.-H., Q. Liu, C. Li, G. Wu, J. Steyaert, and N. A. Lambert. 2015. BRET evidence that β2 adrenergic receptors do not oligomerize in cells. Sci. Rep. 5:doi:10.1038/srep10166.
29. Mercier, J.-F., A. Salahpour, S. Angers, A. Breit, and M. Bouvier. 2002. Quantitative assessment of β1-and β2-adrenergic receptor homo-and heterodimerization by bioluminescence resonance energy transfer. J. Biol. Chem. 277:44925-44931.